

EDITORIAL

Open Access



# Preliminary report of field reconnaissance on the 6 February 2023 Kahramanmaras Earthquakes in Türkiye

Kongming Yan<sup>1,2</sup>, Masakatsu Miyajima<sup>3</sup>, Halil Kumsar<sup>4</sup>, Ömer Aydan<sup>5</sup>, Reşat Ulusay<sup>6</sup>, Zhigang Tao<sup>7</sup>, Ye Chen<sup>1</sup> and Fawu Wang<sup>1\*</sup>

## Abstract

On February 6, a successive rupture of major faults in the Eastern Anatolian Fault Zone and Cardak-Surgu fault triggered a strong mainshock ( $M_w$  7.7) and a major aftershock ( $M_w$  7.6) in Kahramanmaras. The successive earthquake sequence hit southern provinces in Türkiye and northern regions in Syria, causing severe fatality and economic loss. After the earthquakes, the International Consortium on Geo-disaster Reduction (ICGdR) organized an investigation team, involving specialists from China, Japan and Türkiye, to conduct a primary field reconnaissance on seismic damage of infrastructure and ground failures. The 10-day reconnaissance, including a mini-symposium at the Istanbul Technical University (ITU), was conducted from 25 March to 3 April and specifically focused on fault ruptures, liquefaction, landslide, rockfall and lateral spreading along the major ruptured faults from Antakya in Hatay to Goksun in Kahramanmaras, passing through provinces of Gaziantep, Adiyaman and Malatya. By this reconnaissance, a large amount of original seismic data was collected and a primary understanding was established for further steps on mitigation and reduction of seismic damages and its secondary geohazards.

**Keywords** Field investigation, Kahramanmaras earthquakes, Seismic damage, Liquefaction, Ground failure

## Introduction

At 04:17 (GMT +3) on February 6, a strong earthquake ( $M_w$  7.7) occurred at Pazarcik in Kahramanmaras (37° 17' 17" N, 37° 02' 35" E) with a focal depth of 8.6 km (AFAD). About 9 h later, at 13:24 (GMT +3), another earthquake named Ekinozu with a moment magnitude of 7.6 and a focal depth of 7.0 km struck the Elbistan (38.089° N, 37.043° E) in Kahramanmaras and ruptured Cardak-Surgu fault, which is entirely different from East Anatolian Fault Zone (Aydan and Ulusay 2023). The Pazarcik earthquake was initiated at the Dead-Sea Fault and triggered the East Anatolian Fault Zone (EAFZ), one of two major active fault zone in Türkiye. The distance between two epicentres was 95 km.

This event caused widespread damage and massive fatalities. The mainshock caused a maximum Mercalli intensity of XII (extreme) in the city centre of Antakya, the capital of Hatay Province. The earthquakes caused a

\*Correspondence:

Fawu Wang

wangfw@tongji.edu.cn

<sup>1</sup> Department of Geotechnical Engineering, College of Civil Engineering, Tongji University, Shanghai, China

<sup>2</sup> Disaster Prevention Research Institute, Kyoto University, Kyoto, Japan

<sup>3</sup> Institute of Science and Engineering, Faculty of Environmental Design, Kanazawa University, Kanazawa, Japan

<sup>4</sup> Earthquake Science and Engineering Institute, Department of Geological Engineering, Pamukkale University, Denizli, Turkey

<sup>5</sup> Department of Civil Engineering and Architecture, Ryukyu University, Okinawa, Japan

<sup>6</sup> Department of Geological Engineering, Hacettepe University, Ankara, Turkey

<sup>7</sup> State Key Laboratory of Geomechanics and Deep Underground Engineering, China University of Mining and Technology (Beijing), Beijing, China

confirmed death toll of 50,783 and 107,000 reported injuries according to the Ministry of Interior of the Republic of Turkey until 18 May 2023 (IBC report 23, 2023).

The catastrophic 2023 Kahramanmaras earthquakes were triggered by a rupture along the Narli segment of Dead-Sea Fault and two lateral strike-slip segments (Pazarcik and Amanos segments) belonging to the EAFZ. If the displacement of the faults was densely monitored before their final ruptures, it would effectively reduce the damage and casualties because of on-time prediction. In this case, how to predict the displacement of the active fault is a challenging scientific problem (e.g., Aydan 2023, Chapter 10). For such a problem, the International Consortium on Geo-disaster Reduction (ICGdR) developed an International Correlation Research Program (ICRP) of “Cross-Fault Measurement for Earthquake Prediction”.

In order to improve and test the possibility of the new technologies for monitoring fault movement, Prof. Manchao He who is director of the ICRP program proposed the field reconnaissance on the 2023 Kahramanmaras earthquakes. The field reconnaissance aimed to collect original data on the ground ruptures and their secondary damages, which would be fundamental research for the next step on conduction of the possible monitoring technologies.

## Overview of the field reconnaissance

### Organizer and investigators

This field reconnaissance was organized by the ICGdR. The reconnaissance team was led by Prof. Fawu Wang

(President of the ICGdR and professor at Tongji University) and Prof. Masakatsu Miyajima (Director-General of the ICGdR and professor at Kanazawa University). The major reconnaissance schedule and contact work in Türkiye was organized by Prof. Halil Kumsar who is the director of Earthquake Science and Engineering Institute, the Department of Geological Engineering, Pamukkale University. Prof. Zhigang Tao (China University of Mining and Technology (Beijing)) and Prof. Ömer Aydan (University of the Ryukyus), joined this field reconnaissance as the secretary general and the major expert of the ICRP, respectively. Moreover, Prof. Reşat Ulusay (President of ISRM) and Dr. Kongming Yan (postdoctoral researcher at Tongji University) joined the field reconnaissance as well. After a 9-day field reconnaissance from Hatay to Kahramanmaras, a mini-symposium was organized by Prof. Remzi Karagüzel at Istanbul Technical University (ITU) on 3 April, 2023 (Fig. 1).

### Field route

The field reconnaissance was conducted from the southern end of Hatay Province to Gökşun in Kahramanmaras Province for 9 days from 25 March to 2 April, as shown in Fig. 2. The route was planned along the east Anatolian fault in the southeast Türkiye. The field reconnaissance team visited representative areas including strong motion, liquefaction, ground surface ruptures, slope failures and the sites of major infrastructures along the faults. The liquefaction mainly occurred in Antakya, Iskenderun and Golbasi. The first two are coastal cities in



**Fig. 1** Group photo of the investigators of the 2023 field reconnaissance in Türkiye. The members (left to right) are: Zhigang Tao, Fawu Wang, Ömer Aydan, Masakatsu Miyajima, Halil Kumsar, Reşat Ulusay and Kongming Yan. The photo was taken by Ilyas at the Titus Tuneli, Hatay

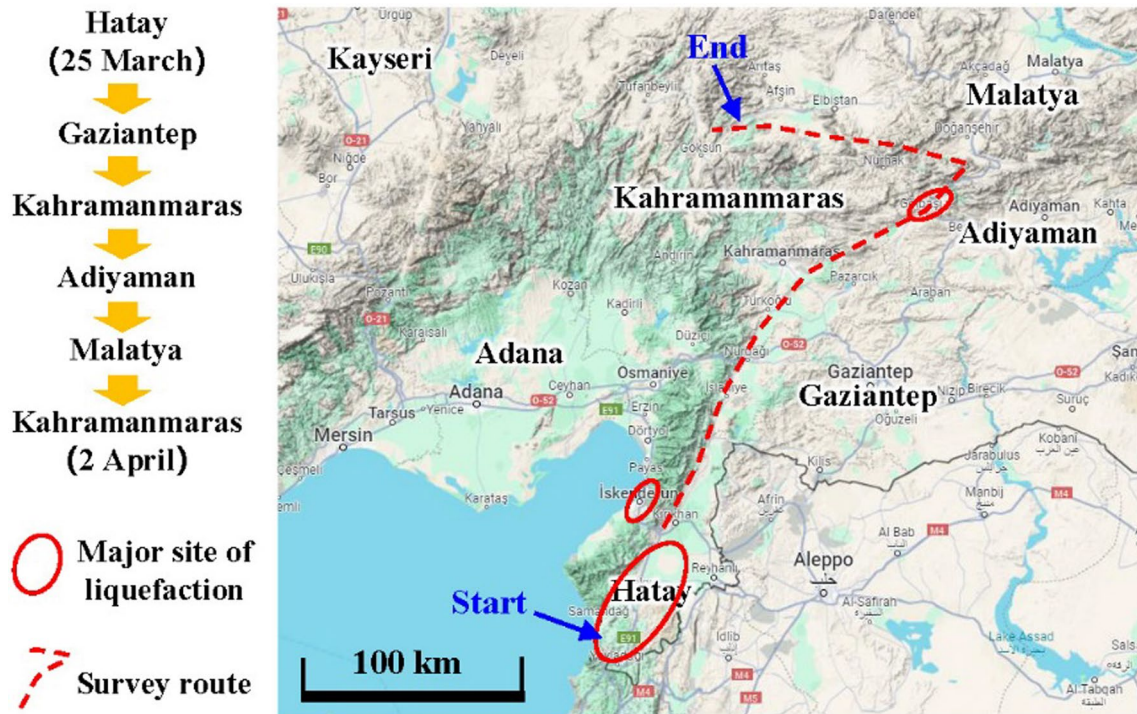


**Fig. 2** Route of the field reconnaissance from Hatay to Kahramanmaras (the base map is captured from Google Maps)

Hatay while the last one is a lakeside region. Moreover, massive liquefaction and its secondary lateral spreading occurred along the rivers.

**Primary investigated results**

**Seismic effect**

According to the preliminary field reconnaissance, the massive damage of buildings due to strong motion and high intense shaking occurred at the city centre of Antakya as shown in Fig. 3a, but not in Kahramanmaras where only several buildings were destroyed by the earthquakes in its old downtown areas as shown in Fig. 3b. In

the Antakya, most of the buildings were destroyed and removed when the reconnaissance team arrived about 50 days later. Major city functions were entirely paralyzed, including transportation, water and electricity supply.

**Damage of infrastructures**

The 2023 Kahramanmaras earthquakes caused severe damage to various infrastructures, including tunnel, life-line facilities, railway, bridge, factory, dam, mosque, historical buildings, hospital, power plant and substations, as shown in Figs. 4, 5, 6, 7.



**Fig. 3** Strong-motion-induced building damage in downtown Antakya (a) and Kahramanmaras (b)

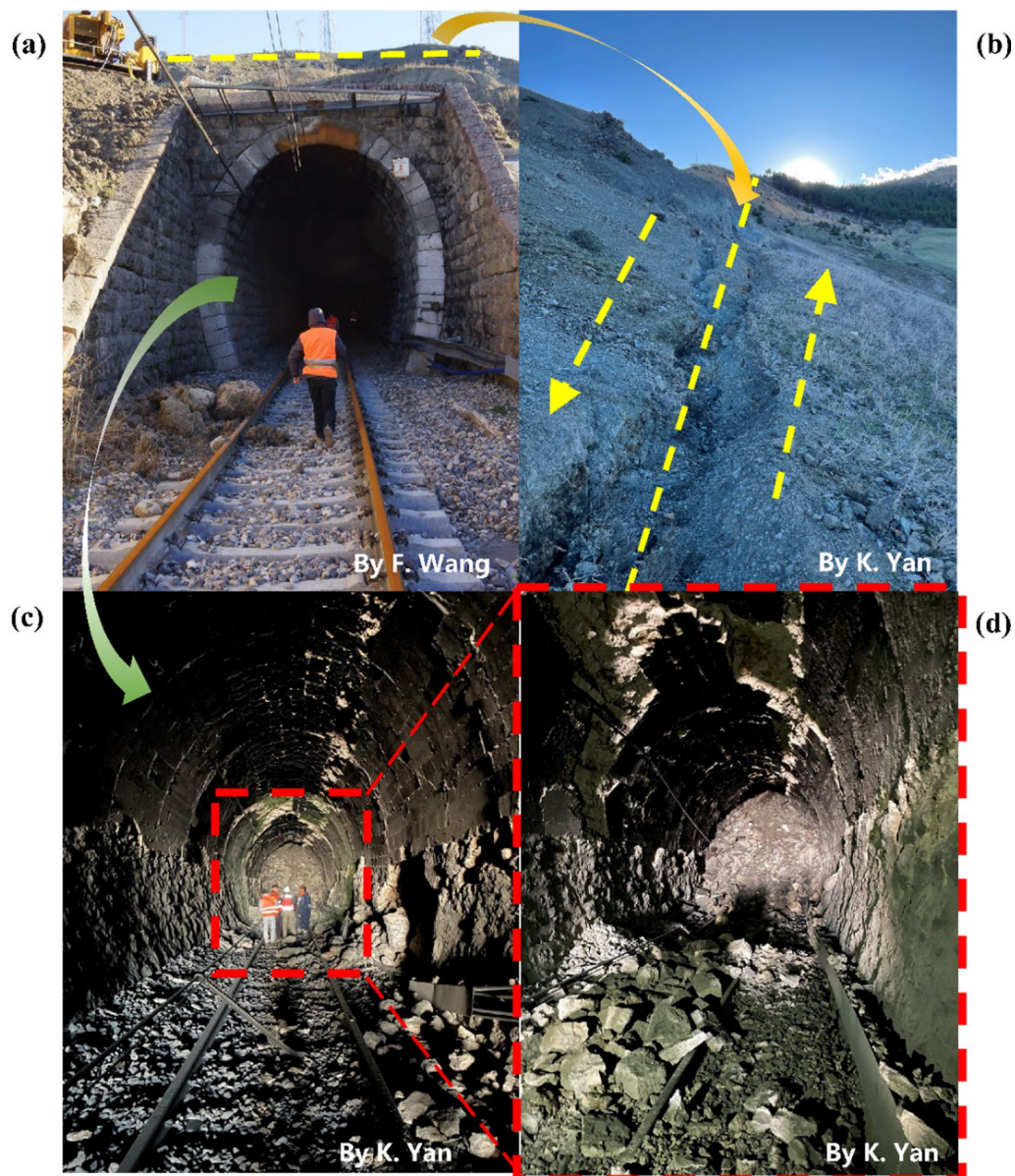


**Fig. 4** A railway tunnel (a) was cut by the left-lateral strike-slip fault (b) in Ozan, causing the tunnel collapsed (c) and the railway line interrupted (d). The railway was still in use before the earthquake

The most severely damaged tunnel was a railway tunnel at Ozan in Golbasi, Adiyaman Province, Turkiye (Fig. 4a). The tunnel was cut by the Erkenek fault segment (Fig. 4b) and was entirely blocked by a rupture-induced collapse inside the tunnel (Fig. 4c, d). The railway tunnel had been still available before the earthquakes. Moreover, there were three explosion sites of natural gas pipeline crossing the fault and cut by the ground rupture, two of the cases occurred in Turkoglu,

Kahramanmaras were shown in Fig. 5 as examples. According to the field investigation, the explosion diameters of the two explosions were estimated to be about 200 m. The two buckled pipelines at Ceceli had a diameter of 1 m and a pipe thickness of 15 mm. The buckling angle was measured to be 30° and 18° respectively, as shown in Fig. 5b. In addition to underground structures, such as tunnels and pipelines, various buildings were also severely damaged as shown in Figs. 6, 7.

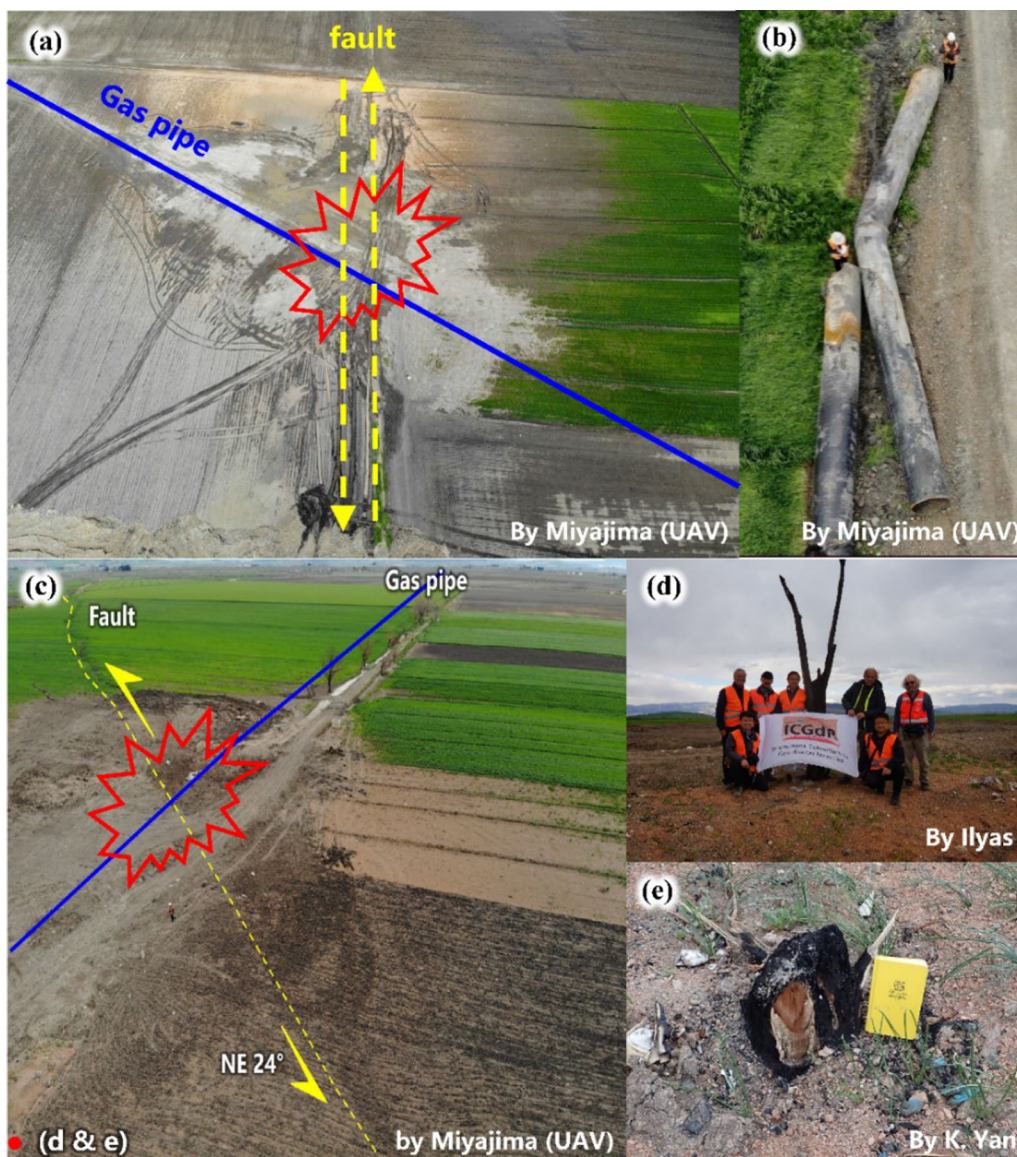


**Fig. 5** Explosions caused by damages of natural gas pipeline crossing the faults in Turkoglu, Kahramanmaraş. **a** Gas pipeline damages at Ceceli and **b** curved steel pipe with an outer diameter of 1 m and a thickness of 15 mm; **c** gas pipeline damages at Golluhuyuk with **d** burnt tree trunks and **e** stumps

### Ground ruptures

In addition to the collapses of buildings, strong seismic effects were illustrated by massive ground surface ruptures caused by fault movement, as shown in Fig. 8. The obvious ground surface rupture first occurred at the north end of Antakya (Fig. 8a) and disappeared at the west end of the second failed fault (Fig. 8b–d). Moreover, massive ruptures crossed through farmland and villages,

triggered subduction and transport line interrupted as shown in Fig. 8e–g.

### Liquefaction and liquefaction-induced ground failures

After the major earthquakes, massive liquefaction and its secondary ground failures in various places were investigated along the main faults (Fig. 9). Four major regions suffered severe liquefaction damage were investigated in

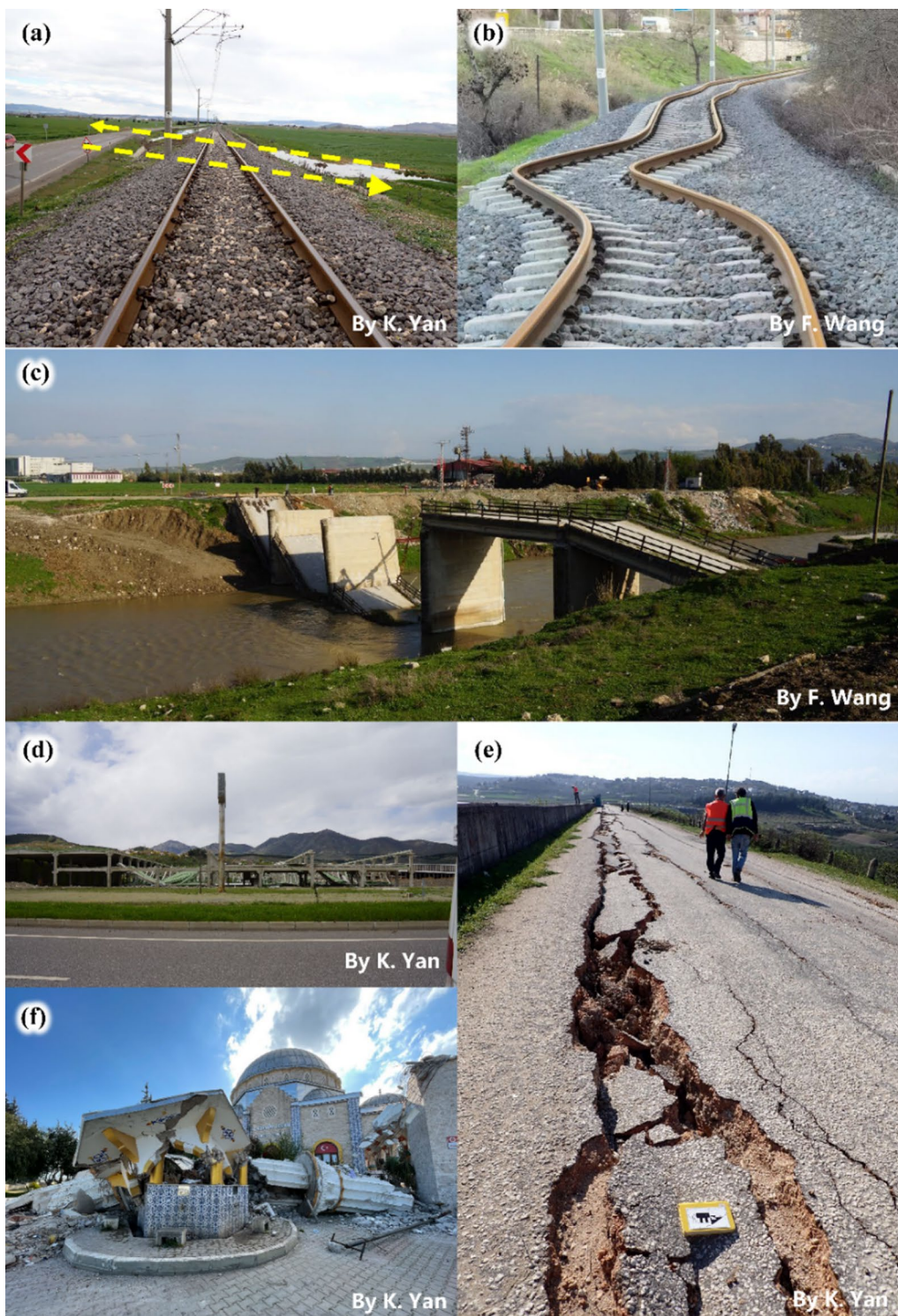


**Fig. 6** Seismic damages of major infrastructures, including **a** & **b** railways, **c** bridge, **d** factory, **e** Yarseli dam and **f** mosques



**Fig. 7** Seismic damages of major infrastructures, including **a** & **b** Gaziantep castle, **c** & **d** Hatay Hospital, **e** power plants and **f** substations and **g** provincial council building of Hatay (about 100 years old)

this reconnaissance as circled in red in Fig. 9. The liquefaction mainly occurred at coastal regions (Samandag and Iskenderun in Hatay), riverside areas (Demirköprü in Hatay and Cumhuriyet in Adiyaman), lakeside area (Golbasi in Adiyaman) and some fault rupture surface (Kumlu in Hatay), as shown in Figs. 10, 11 and 12.

The major characteristics and damage of liquefaction include sandboiling in farmland and wheat field (Fig. 10a, b), ground cracks on road (Fig. 10c), subduction (Fig. 10d, f), floating upward of sewer manhole (Fig. 10e), uneven deformation (Fig. 10g, h) and massive lateral spreading along rivers (Figs. 11, 12) and lakeshore

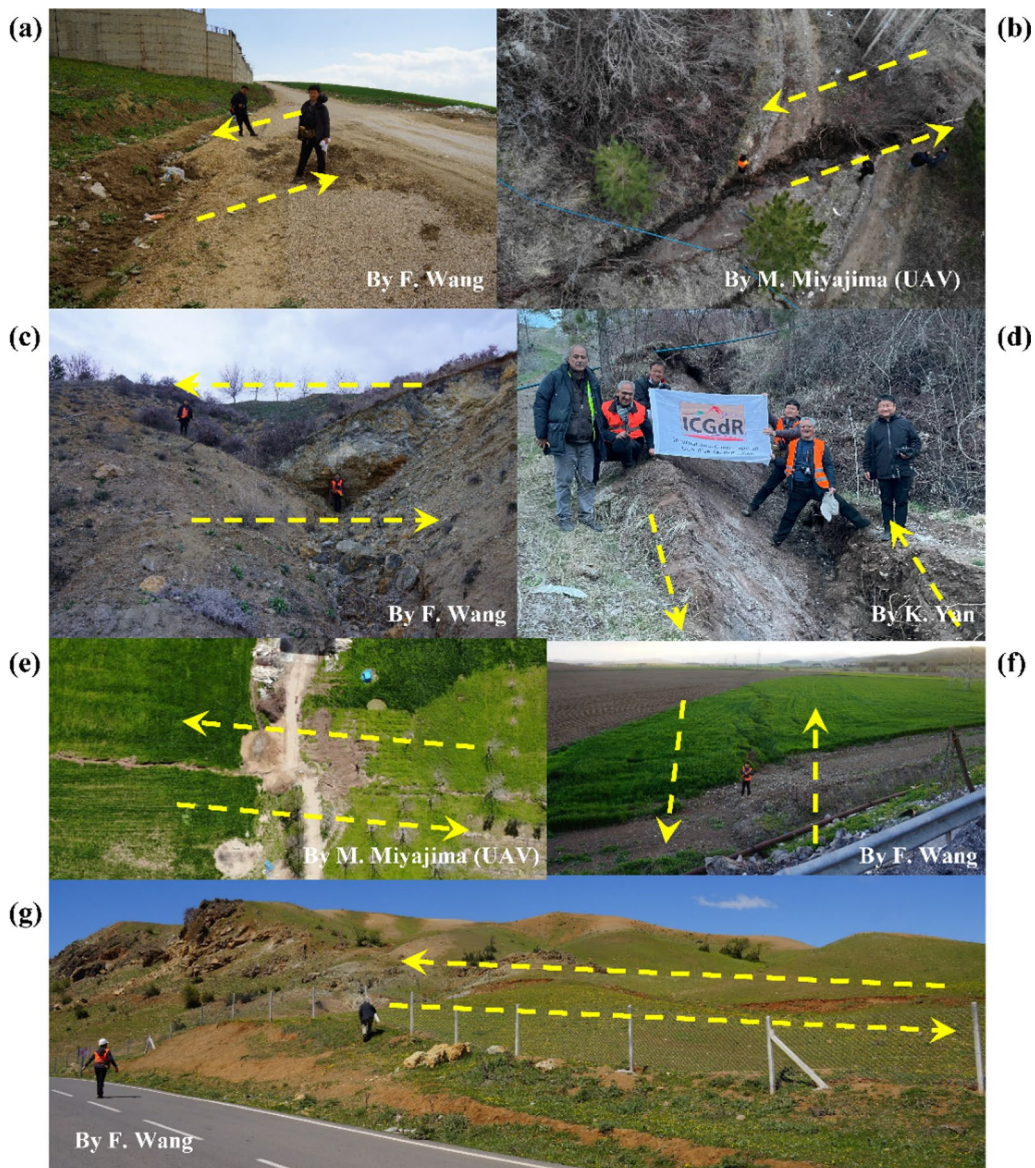


**Fig. 8** Ground ruptures along the investigated faults at **a** Kirikhan (36°28'44.7"N, 36°20'01.3"E), **b & d** Findik (38°03'53.9"N, 36°44'12.4"E), **c** İcmeler (38°01'47.6"N, 37°10'08.1"E), **e** Balkar (37°43'48.8"N, 37°33'30.3"E), **f** Güzelyurt (37°28'47.6"N, 37°02'31.7"E) and **g** Tevekkelli (37°27'13.4"N, 36°59'15.8"E)

(Fig. 13). Figure 10a illustrates an orchard of oranges at the coastal region in Samandag was covered by massive sandboiling, while a sandboiling belt was also observed along a long ground rupture at a wheat field in Kumlu as shown in Fig. 10b. The erupted sands were collected as S1 and S3 whose gradation curves were illustrated in Fig. 15 with detailed gradation parameters in Table 1. The S3 was poorly graded compared to S1 although they

had similar median diameter ( $d_{50}$ ). Similarly, massive liquefaction and its secondary damage were investigated at coastal regions surrounding the Lunapark in Iskenderun. In addition to the similar sandboiling as Fig. 10a, massive liquefaction-induced damage on infrastructure (like road, port) and collapse of high-story resident buildings, causing enormous fatality and economic loss. The same liquefaction-induced damages (Fig. 10f–h) occurred

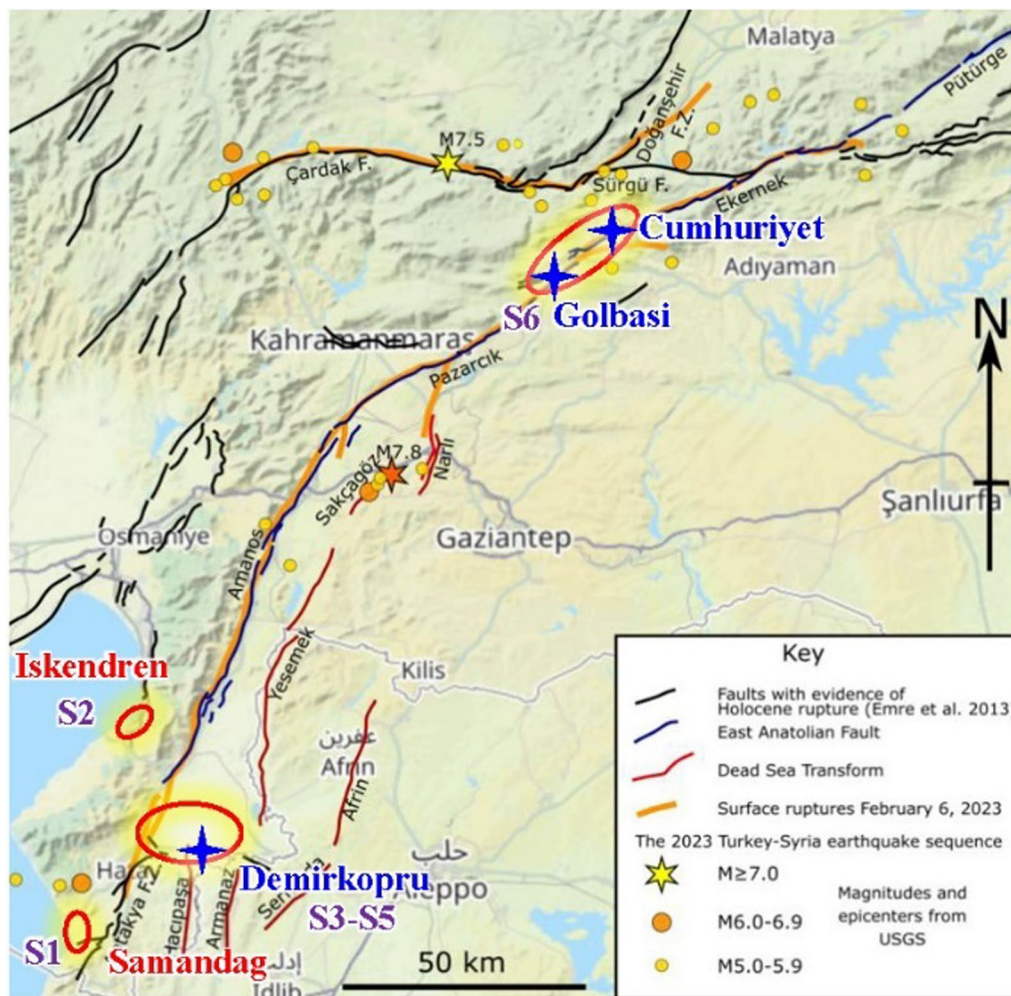


**Fig. 9** Distribution of investigated liquefaction sites (based on Mike Norton 2023)

in the downtown Golbasi which is located close to the Golbasi Lake. Compared to the S1 and S3, the liquefied sand in Iskenderun was finer and poorly graded, with a median diameter of 0.17 mm and a smaller uniformity coefficient of 1.78. It is slightly different from the S6 samples collected from Golbasi, which is much coarser ( $d_{50}=0.49$  mm) and has a similar gradation with the S1.

Different from the above liquefaction damage, the lateral spreading usually occurred at topographically uneven regions, like riverside and lakeshore regions as shown in Figs. 11, 12, 13. A riverside region at Demirkopru was investigated with four parts of liquefaction-induced lateral spreading as shown in Fig. 11. In Part A, a lateral

spreading to an orchard field (Fig. 11d) caused a severe broken over 1 km of the Antakya Cilvegözü Yolu which is a significant transport way in Hatay as shown in Fig. 11c. On the opposite side of the road, a large area of farmland was destroyed by the lateral spreading (Fig. 11e) with enormous explosive sand volcanoes at ground cracks (Fig. 11f, g). Moreover, the lateral spreading at Parts C and D destroyed a primary school, several resident buildings and a cemetery as shown in Fig. 11h, i. In this liquefaction site, two kinds of samples were collected at the roadside orchard (S4) and opposite side of the cemetery (S5). The S4 has similar size distribution features compared to the S1, S3 and S6, but different from S5. The S5



**Fig. 10** Sandboiling and subduction triggered by liquefaction. **a–e** are liquefaction sites at coastal areas at Samandag and Iskenderun Lunapark, while **f–h** are the lakeside area at downtown Golbasi (Photos were taken by K. Yan)

was much finer ( $d_{50}=0.07$  mm) compared to the other samples but well graded with a large uniformity coefficient of 7.38 ( $>5.0$ ) and a coefficient of curvature of 2.08 (ranging in 1.0–3.0), which represents it might be difficultly liquefied compare to the other poorly-graded sands. In this case, the liquefaction of S5 might represent the strong capacity of the Kahramanmaraş earthquakes on liquefaction in this region. Moreover, similar lateral spreading at riverside regions triggered slope failure, ground displacement and road collapse at a riverside

area close to a small dam at Cumhuriyet in Adryaman (Fig. 12).

In the severely liquefied downtown of Golbasi, a lake-shore campus of the Adiyaman Üniversitesi Gölbaşı Meslek Yüksek Okulu located close to the Golbasi Lake was destroyed by the liquefaction-induced lateral spreading as shown in Fig. 13. In the campus, a large area of land with several buildings slid to the Golbasi Lake and caused the buildings submerged (Fig. 13a, d) and collapsed (Fig. 13e).



**Fig. 11** Liquefaction-induced lateral spreading (a) at Demirköprü (b) in Hatay. The Part A damaged the road (c) by the lateral spreading to a roadside wheat field (d); The Part B laterally moved to the river (e) with massive sand volcanoes (f) and ground cracks (g) in the riverside farmland; The Part C and Part D damaged a primary school with several resident buildings (h) and a cemetery (i)

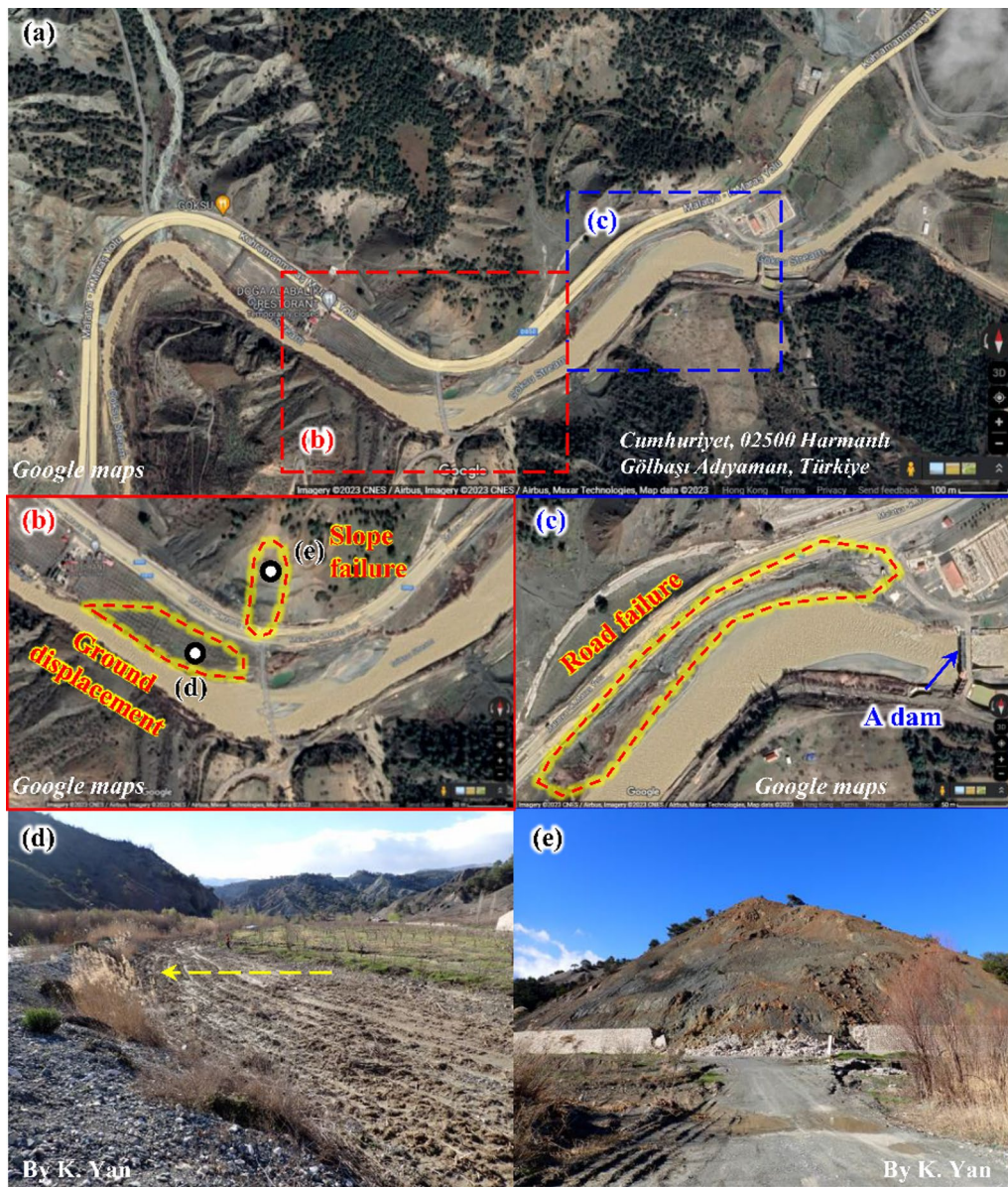


**Fig. 12** Liquefaction-induced lateral spreading at Cumhuriyet in Adyaman (a), causing a riverside ground displacement (b & d) with a slope failure (b & e) and a road failure (c) along the river

In this field reconnaissance, six liquefaction samples, involving coastal, riverside and lakeside regions and fault rupture zone, were collected from Samandag to Golbasi as shown in Figs. 9, 14. Detailed information on gradation parameters of the samples with the sampling location was listed in Table 1. According to grain sieve analysis for the six samples (Fig. 15), most of the samples were poorly

graded and coarser compared to the S5 collected at a riverside farmland in Demirköprü, Hatay.

**Slope failures**

In addition to liquefaction-induced lateral spreading, several slope failures and massive small-scale rock-falls were directly triggered by the strong earthquakes

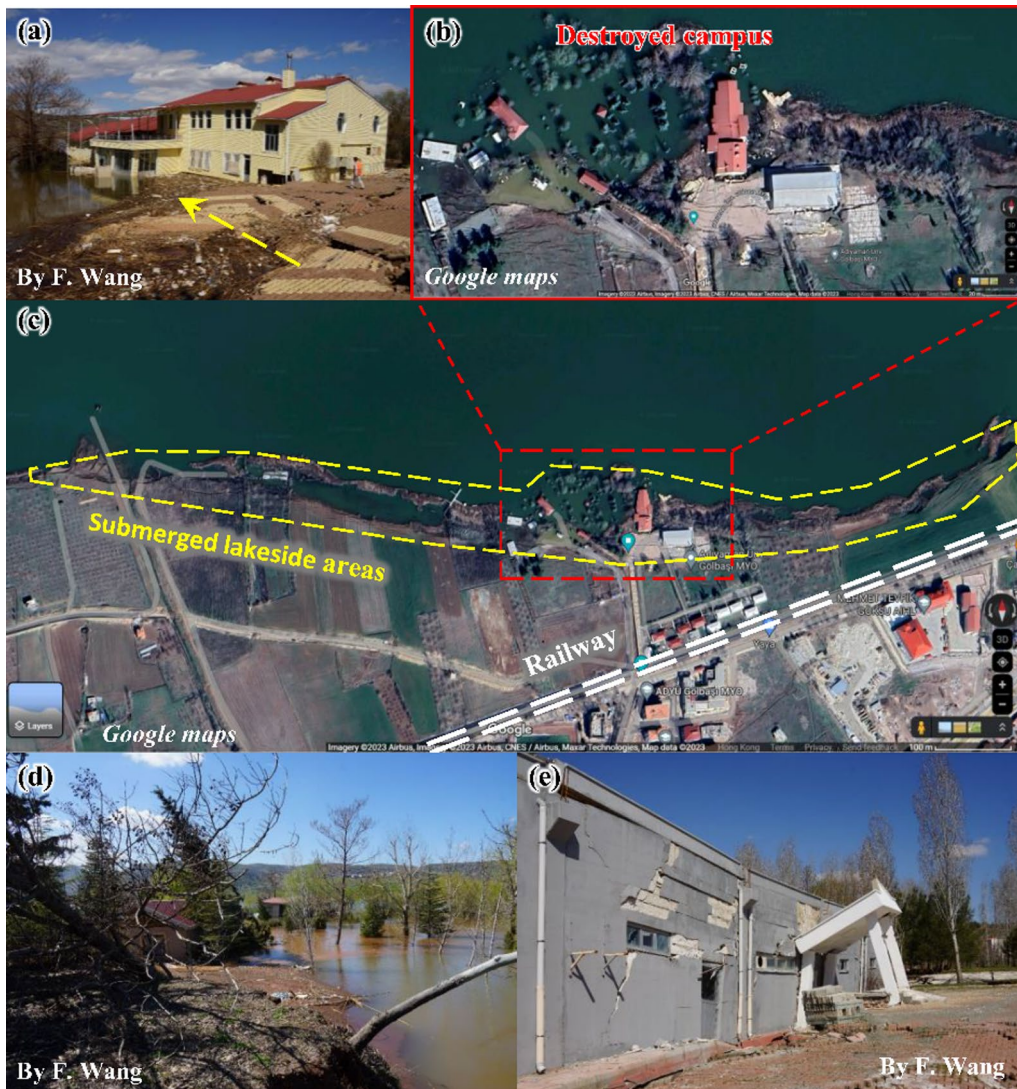


**Fig. 13** Liquefaction-induced lateral spreading at the lakeside area (c) of the Golbasi Lake, causing several buildings submerged (a, b & d) by the lake and damaged (e) by uneven subduction

**Table 1** Detailed features of the major liquefaction samples

No	Median diameter ( $d_{50}$ /mm)	Uniformity coefficient ( $C_u$ )	Coefficient of Curvature ( $C_c$ )	Sampling location
S1	0.32	5.50	0.87	36°03'28.1"N 35°58'12.1"E An orchard of oranges at Samandag, Antakya, Hatay
S2	0.17	1.78	0.97	36°35'28.7"N 36°10'45.2"E The coastal Lunapark in Iskenderun, Hatay
S3	0.37	2.7	1.19	36°21'23.6"N 36°23'35.0"E A wheat field at Kumlu, Hatay
S4	0.34	3.05	0.95	36°14'43.3"N 36°21'44.4"E An orchard by the Antakya Cilvegözü Yolu at Demirköprü, Hatay
S5	0.07	7.38	2.08	36°14'53.6"N 36°21'18.9"E A riverside farmland at Demirköprü, Hatay
S6	0.49	5.29	0.98	37°47'22.3"N 37°38'19.5"E TCDD Golbasi train station in Adiyaman



**Fig. 14** Dried samples (a-f) from major liquefaction sites with detailed information listed in Table 1

and identified in this field reconnaissance, as shown in Figs. 16 and 17. In particular, a group of slope failures occurred along the rupture zone of the fault at Yeni, Şekeroba, Türkoğlu in Kahramanmaraş Province, as shown in Fig. 16. Moreover, there were massive slope failures nearby the faults, including the Islahiye Landslide (Fig. 18) and Tepehan Landslide (Fig. 24). The Islahiye landslide was located in a formation consisting of dolomite and dolomitic limestone and was close to two fault segments. The Tepehan Landslide was due to a planar sliding of mudstone formation dipping with a gentle

angle of 10°. Both of the two landslides had a strong spatial relationship with the fault zones as well as the effect of geological settings.

The Islahiye landslide, directing to 135° with an estimated slope of 35° as shown in Fig. 18, had a maximum horizontal runout of 506 m and a vertical drop of 234 m from scarp top (Point A) to the deposit front (Point C), forming a fan-shaped deposition with a maximum width of 355 m (D-E). The landslide, with an exposed main scarp of about 100 m high, occurred in a valley (Fig. 19) and formed a 94-m-wide barrier lake (Fig. 18b), interrupting the road from Idilli to Degirmencik. At toe of the debris deposition, a spillway of the barrier lake was constructed at about 20 m above the lake bottom (Fig. 18b, d).

The Islahiye landslide is located between two minor fault segments, 1.8 km from the south end of Islahiye segment and about 0.6 km from the north end of the Hassa segment (Fig. 19), according to geological information from general directorate mineral research and exploration directed by Mehmet UZER. From the pre-landslide image (Fig. 19a), a large area of excavation existed at mount peak of the slope. According to local contour map (Fig. 20), based on data from the Open-TopoMap, the landslide dropped from an altitude of 900 m above sea level (a.s.l.) to 639 m a.s.l. at the valley

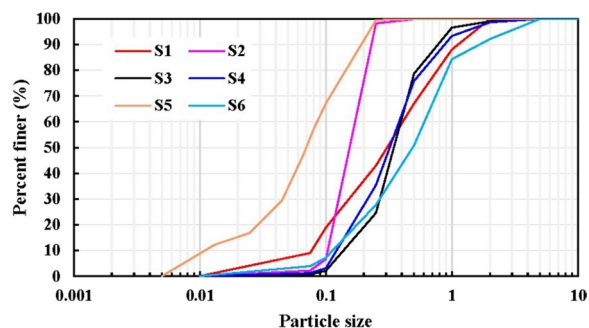


**Fig. 15** Grain size distribution curves of the investigated liquefaction samples

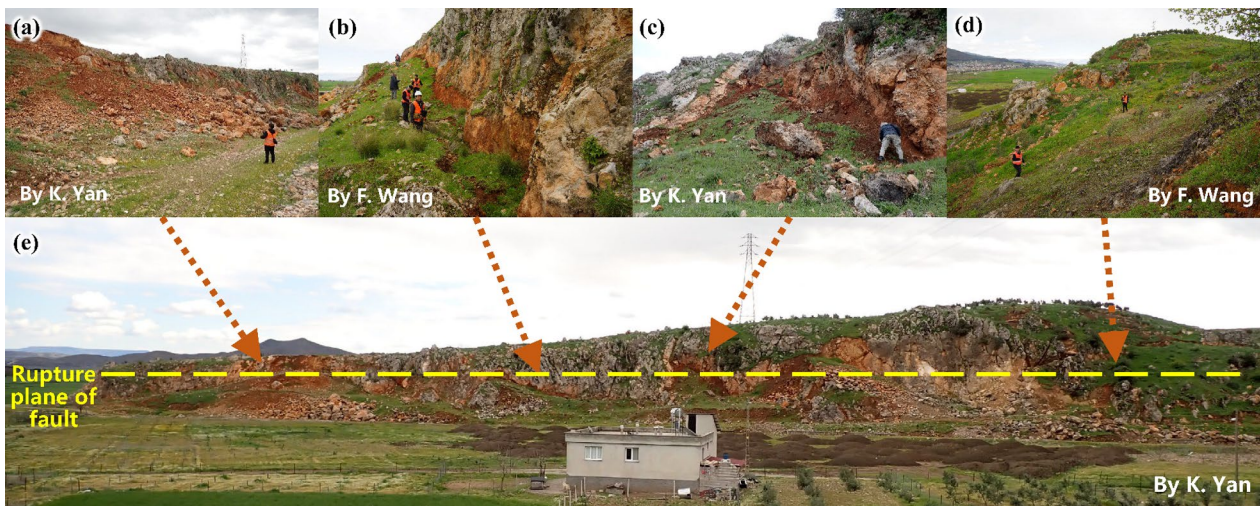


**Fig. 16** Fault-triggered slope failures and collapses. **a-d** illustrate major features along the rupture plane **e** of fault



**Fig. 17** Slope collapses and rockfalls along the road at **a** Sakçagözü (37°10'35.6"N, 36°55'54.5"E), **b** Tiyek (36°48'20.9"N, 36°29'27.5"E), **c** & **d** Olucak (37°10'44.9"N, 36°42'36.3"E)

bottom. The landslide has an estimated sliding surface with a dip angle of 35° and finally reposed at 24.8° according to its longitudinal profile (Fig. 20). Moreover, the landslide is located in a geologically complex region with various lithology and active tectonics, surrounded by minor left-lateral strike-slip faults and overthrusts. The geological map (Fig. 21) suggests that the landslide occurred in a formation of Kurici dolomite involving dolomite and dolomitic limestone between the upper Triassic and the lower Jurassic.

The Islahiye landslide, directly triggered by mainshock of the Kahramanmaraş earthquakes, was just about 3 km away from a seismic station (TK-2718) in downtown of Islahiye (Fig. 19). In this case, dynamic stress status on the sliding surface could be briefly calculated by a simplified method as shown in Fig. 22 based on the original acceleration records from TK-2718.

The calculation was processed by the Eqs. (1)–(5) according to the procedure from Fig. 22a–c. Firstly, the horizontal acceleration on the sliding direction ( $A_s$ ) could be calculated by Eq. (1) from original acceleration records on horizontal direction of NS and EW. Then, the accelerations perpendicular to and parallel to the sliding surface ( $A_n$  and  $A_t$ ), with a dip angle of  $\theta$ , were calculated by Eqs. (2) and (3) from original vertical seismic component ( $A_{UD}$ ) and extrapolated horizontal acceleration ( $A_s$ ). Finally, combining estimated property of sliding mass, such as unit weight ( $\gamma$ ), density ( $\rho$ ) and depth ( $h$ ), normal and shear stresses on the sliding surface could be extrapolated by the Eqs. (4) and (5), respectively.

$$A_s = A_{EW} \cdot \cos(\alpha - 90^\circ) - A_{NS} \cdot \cos(180^\circ - \alpha) \quad (1)$$

where  $A_s$  is acceleration in horizontal sliding direction,  $A_{EW}$  and  $A_{NS}$  are horizontal components of original

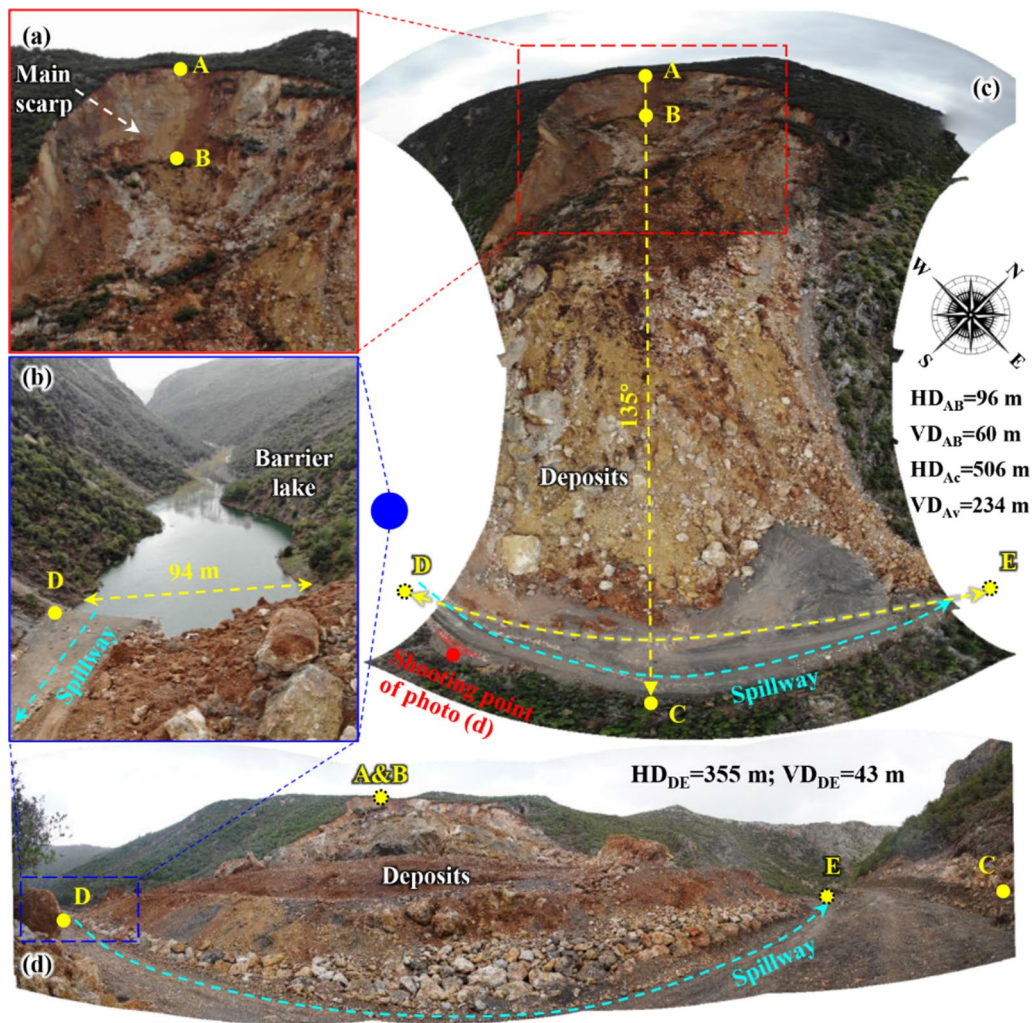


**Fig. 18** Overview of the Islahiye landslide (based on UAV images by Miyajima). The main scarp (a) and barrier lake (b) are illustrated on the panoramas (c & d) of the landslide

acceleration records in North–South and East–West directions respectively,  $\alpha$  is the sliding direction.

$$A_n = -A_s \cdot \sin\theta - A_{UD} \cdot \cos\theta \quad (2)$$

$$A_t = A_s \cdot \cos\theta - A_{UD} \cdot \sin\theta \quad (3)$$

where  $A_n$  and  $A_t$  are accelerations on normal and tangential directions of the sliding surface,  $A_{UD}$  is a vertical component (Up–Down) of original acceleration records,  $\theta$  is dip angle of the sliding surface.

$$\sigma = \gamma h \cdot \cos\theta + \rho h \cdot \cos\theta \cdot A_n \quad (4)$$

$$\tau = \gamma h \cdot \sin\theta + \rho h \cdot \sin\theta \cdot A_t \quad (5)$$

where  $\sigma$  and  $\tau$  are normal stress and shear stresses of the sliding mass on the estimated sliding surface,  $\gamma$  and  $\rho$  are unit weight and density of the sliding mass while  $h$  is the depth of the sliding mass from slope surface to sliding surface.

By above calculation procedure, a simplified dynamic stress path was obtained as shown in Fig. 23i, with time-histories of normal and shear stresses (Fig. 23g, h), and extrapolated acceleration components on sliding direction and sliding surface (Fig. 23c, e, f), from original seismic records at TK-2718 (Fig. 23a, b, d).

Differing from the Islahiye Landslide which failed on a steeper slope, the Tepehan Landslide, with an estimated depth of 25 m, initiated on a gentle bedding slope with a

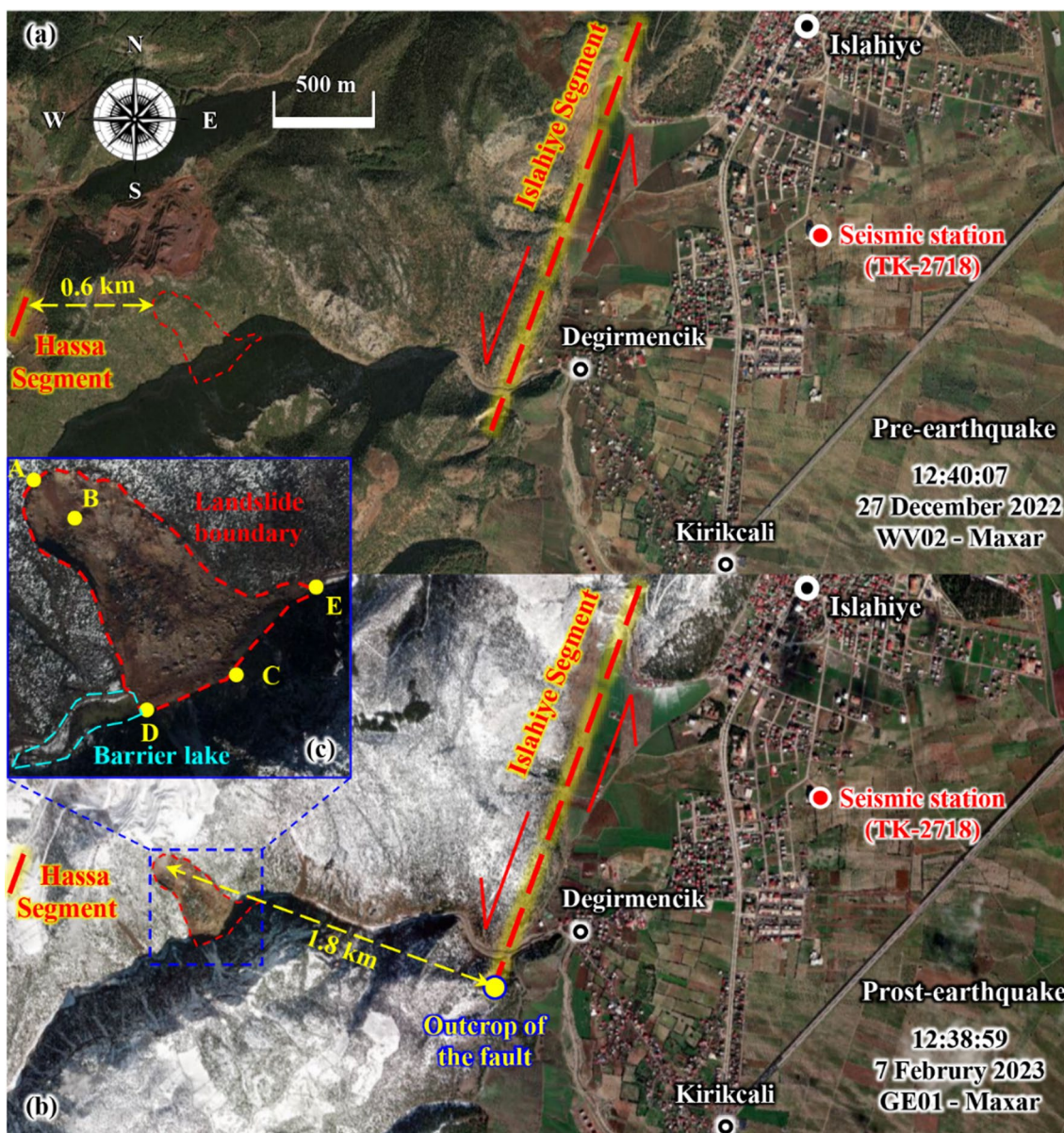


**Fig. 19** Satellite images surrounding the Islahiye landslide (a) before and (b & c) after the earthquakes. The satellite images were collected from OPEN DATA PROGRAM of Maxar (<https://www.maxar.com/open-data/turkey-earthquake-2023>)

dip angle of 10°, as illustrated in Fig. 24. A field investigation in the source area (Fig. 24a, b) revealed that the sliding mass primarily consists of layered fresh mudstone and overlying soils. The mudstone easily disintegrated in the presence of water, as depicted in in-situ image (Fig. 24c) and a simplified slake test in Fig. 24d. In this instance,

whether the slope failed within the mudstone layer or at the interface of bedding layers could be explored through laboratory test, such as ring shear test on the mudstone (Fig. 26). The input dynamic stresses, including normal stress and shear stress (Fig. 25), were estimated based on earthquake records from a nearby seismic station

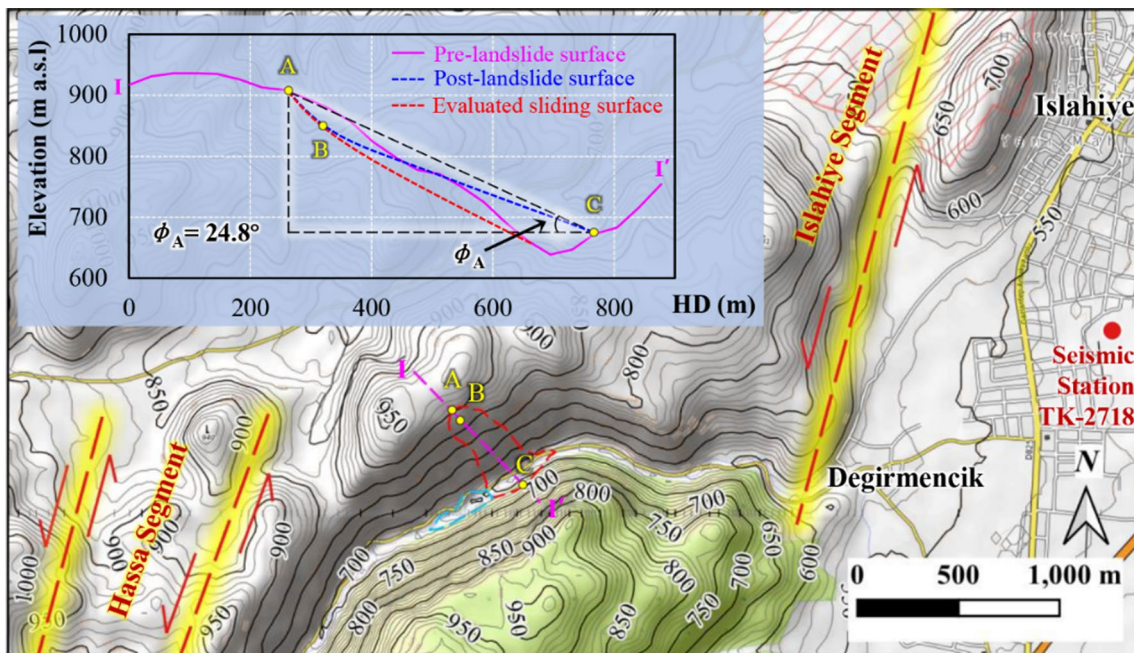


**Fig. 20** Contour map and longitudinal profile variation of the Islahiye landslide (based on OpenTopoMap)

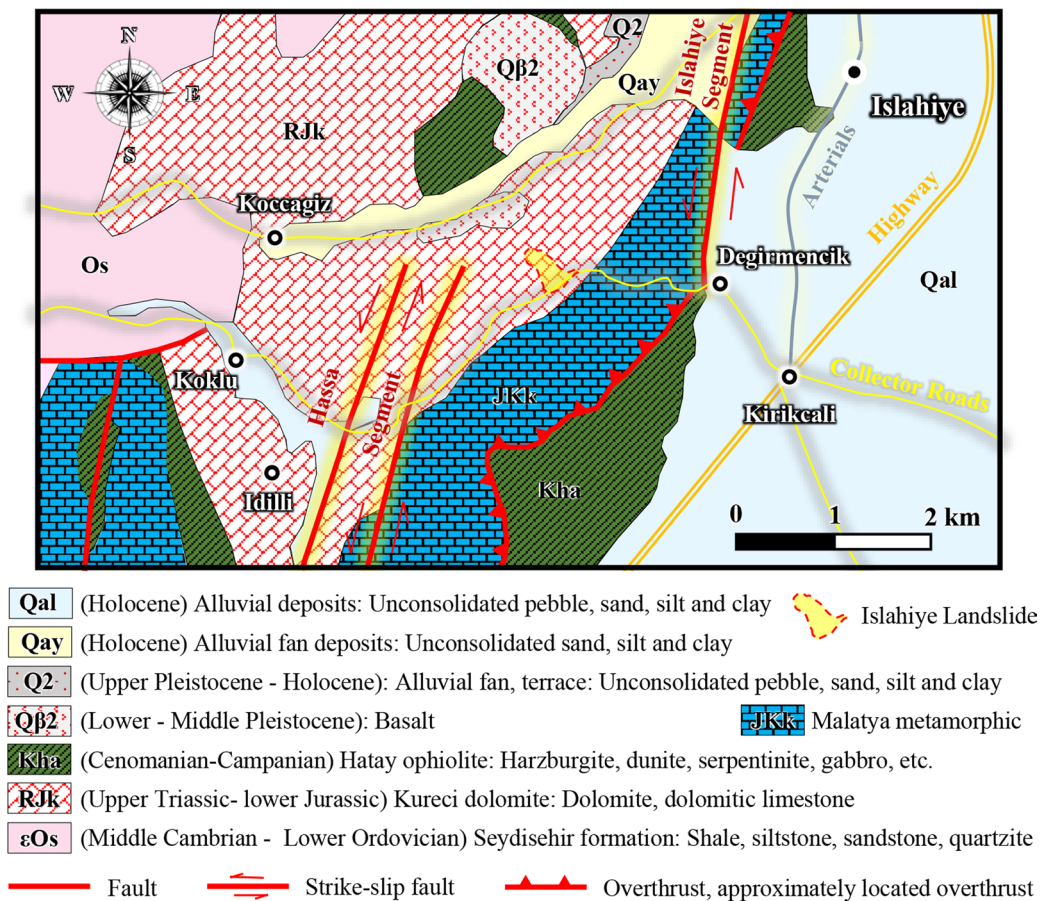


**Fig. 21** Geological settings surrounding the Islahiye landslide (based on general directorate mineral research and exploration directed by Mehmet UZER)

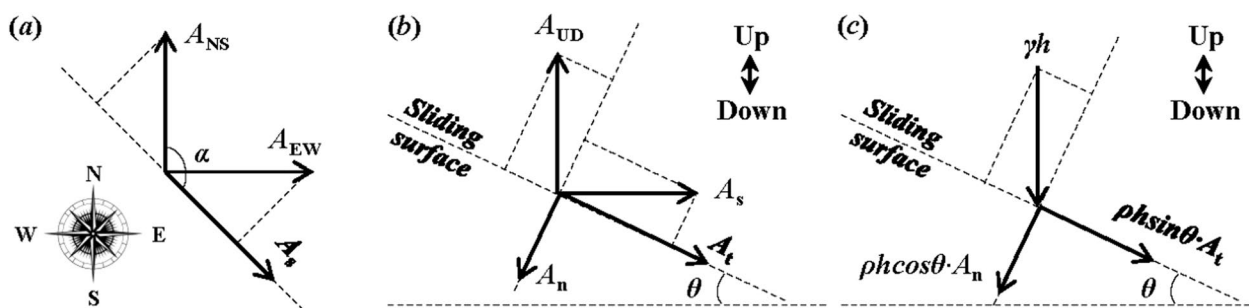


**Fig. 22** Calculation of dynamic normal and shear stresses on the sliding surface by the procedure from (a) to (c)

(TK-3136). The collected mudstone sample was finely crushed (Fig. 26a) and subsequently sheared using the ICL-2 apparatus, as shown in Fig. 26b–d).

The crushed mudstone initially underwent testing in a saturated condition without porewater pressure (Fig. 27a). Both ESP and TSP did not reach the strength line of the saturated sample, suggesting that the mudstone cannot fail under collaborative effect of seismic loading and lower groundwater. Then, increasing the porewater pressure to 250 kPa, representing a high groundwater level even reaching the ground surface, caused the ESP to reach the strength line. This implies that the mudstone could fail under the earthquake loads if the porewater pressure reaches 250 kPa. However, based on the field investigation, there was no high level of groundwater inside the sliding mass. Therefore, the sliding surface of the Tepehan Landslide could not be within the mudstone layer, but might be at the interface of two bedding layers (Fig. 28).

**Mini-symposium at ITU**

After a 9-day field reconnaissance from 25 March to 2 April, all team members returned to Istanbul to visit the Istanbul Technical University (ITU) on 3 April for a brief communication on the investigated work and primary understanding of the 2023 Kahramanmaras earthquakes. The mini-symposium was hosted by Prof. Remzi Karagüzel and consisted of reconnaissance members and several researchers including Emeritus Prof. Dr. Zeki Hasegür at ITU. Prof. Aydan provided a presentation with a brief introduction of the seismic damages and primary data the team collected. Prof. Miyajima presented the aerial videos and photos taken by UAV. After that, the

participants had a brief communication and proposed to organize a formal symposium to communicate the reconnaissance results from different views, like liquefaction, slope failures, and seismicity based on various laboratories on the collected samples.

**Conclusions**

According to the field reconnaissance, the successive earthquake sequence, involving a major aftershock ( $M_w$  7.6), was caused by successive rupture of major faults in the Eastern Anatolian Fault Zone and Cardak-Surgu fault. These earthquakes resulted in severe damage to residential buildings in downtown Antakya, compared to Kahramanmaras which is closer to epicentres of the two major successive earthquakes. Besides, the successive fault movement and the strong ground motion also induced massive ground ruptures or slope failures, including rockfalls and landslides, causing extensive damage on infrastructure, such as farmland, tunnels, railways, highways, and pipelines. Furthermore, the strong ground motions led to liquefaction in coastal, riverside and lake-shore regions, causing massive sandboiling in farmland and wheat fields, ground cracks, subduction, uneven deformation and massive lateral spreading. The Islahiye landslide, featuring a secondary barrier lake, was affected by complex geological environment between Hassa and Islahiye segments. In case of the Tepehan landslide, which initialled on a gentle bedding mudstone slope, it failed and translationally slid on an interface under mudstone layer, rather than within in the mudstone layer. This finding was described on-site investigation as well as confirmed by the ring shear test on saturated mudstone samples.

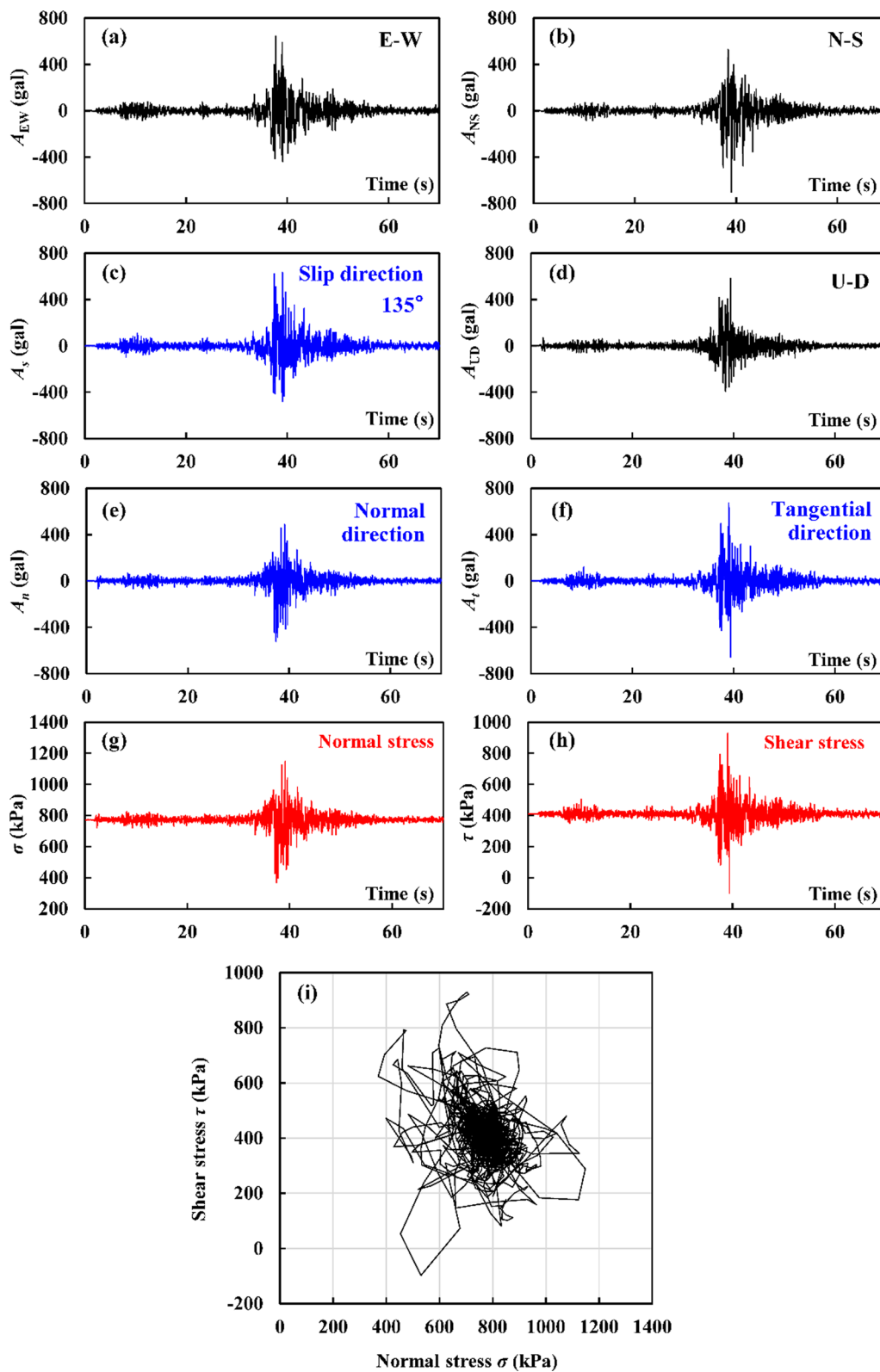


**Fig. 23** Acceleration and stress path on sliding surface based on seismic record from TK-2718. **a, b & d** are original seismic record; **(c)** is acceleration on horizontally slip direction and calculated by **(a & b)**; **e & f** are acceleration on sliding surface in normal and tangential direction, respectively, while **g** and **h** are correspondingly normal and shear stresses which generate the final stress path **i** on the sliding surface

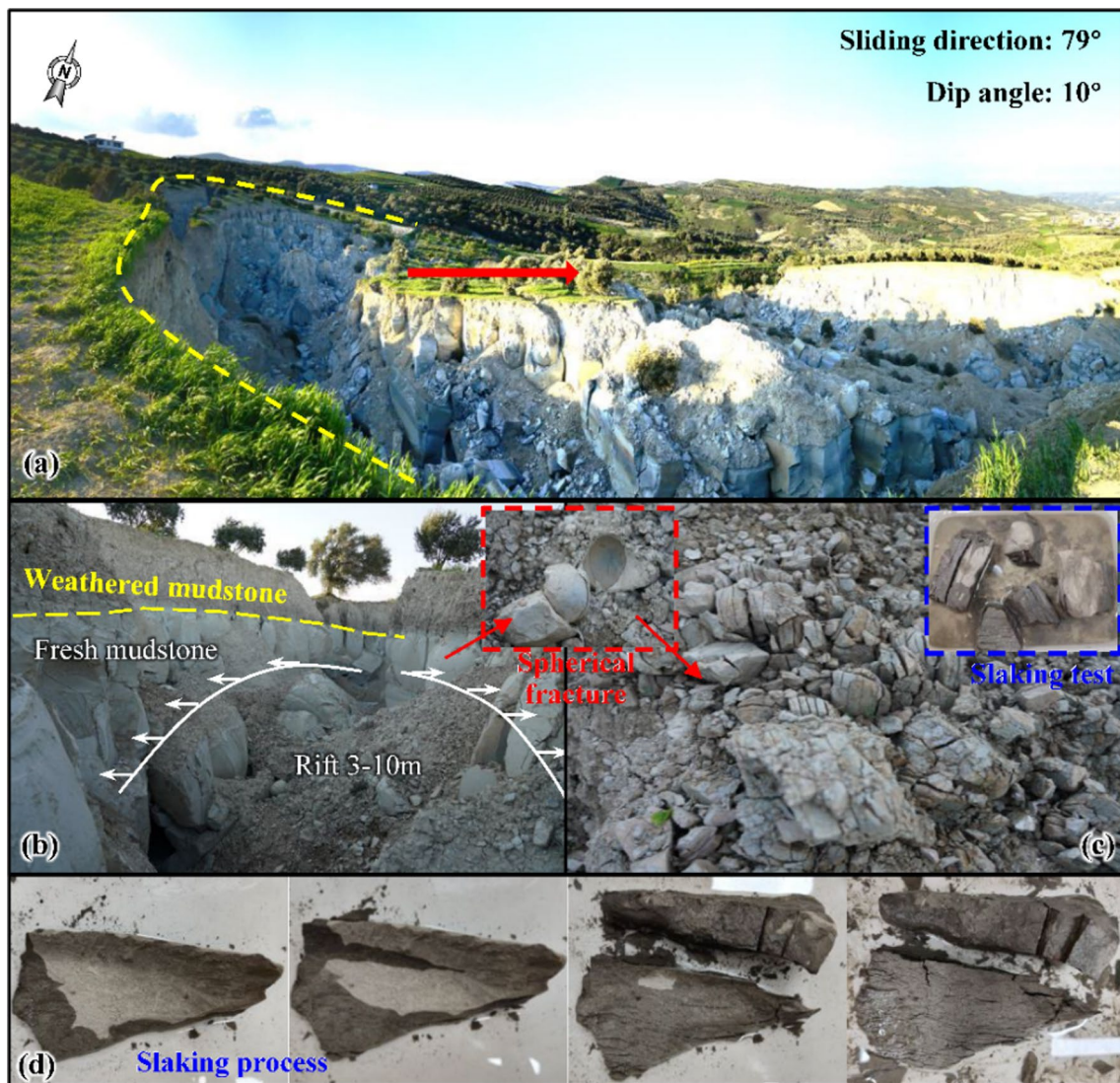


**Fig. 24** Overview of source area (a) and main scarp (b) of the Tepehan Landslide and slaking progress (c & d) of the mudstone

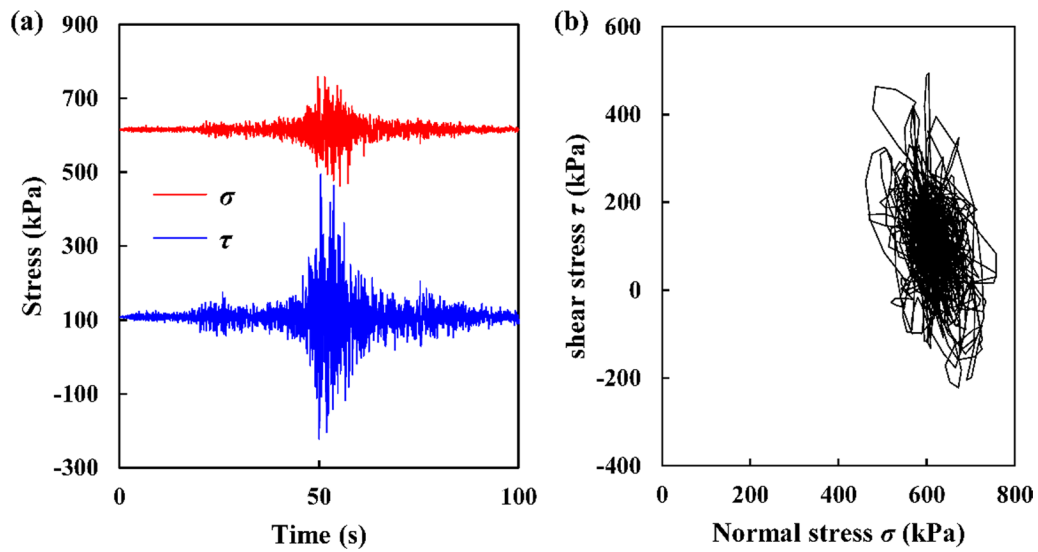


**Fig. 25** Normal and shear stresses (a) and the final stress path (b) on the sliding surface of the Tepehan Landslide based on seismic records by TK-3136

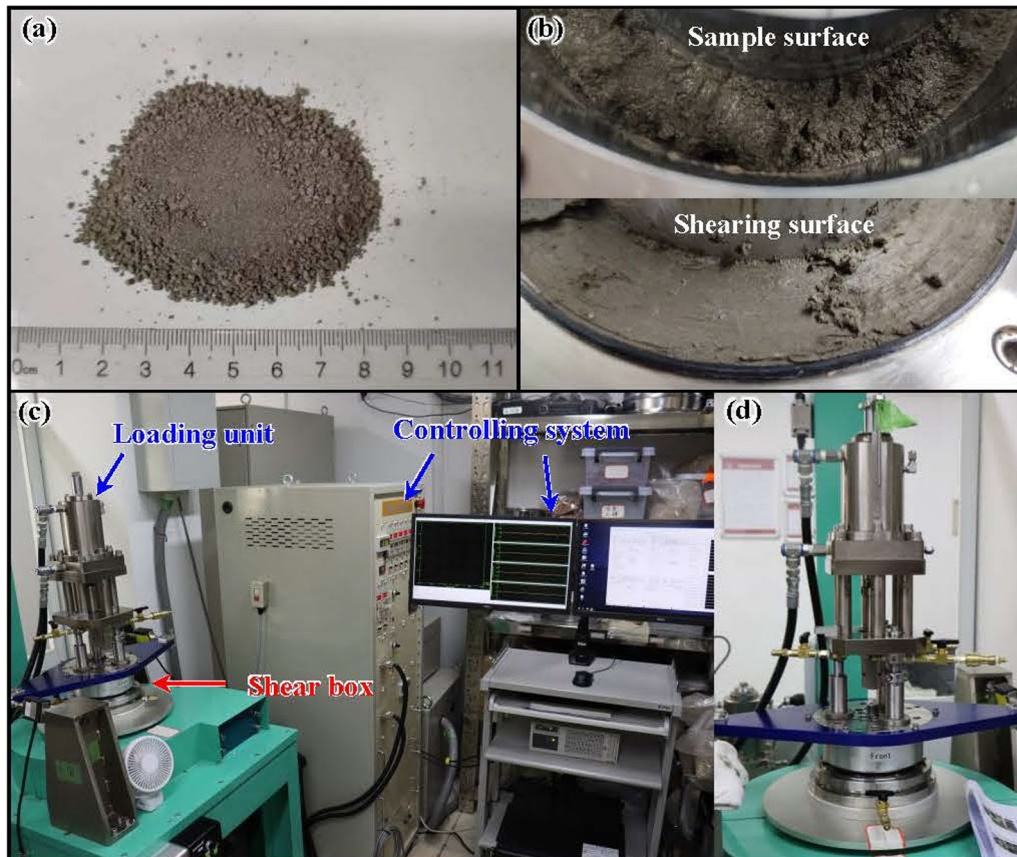


**Fig. 26** Ring shear test on the mudstone sample: **a** Dried and crushed sample; **b** Sheared sample after test; **c** ICL-2 ring shear apparatus and **d** shear box

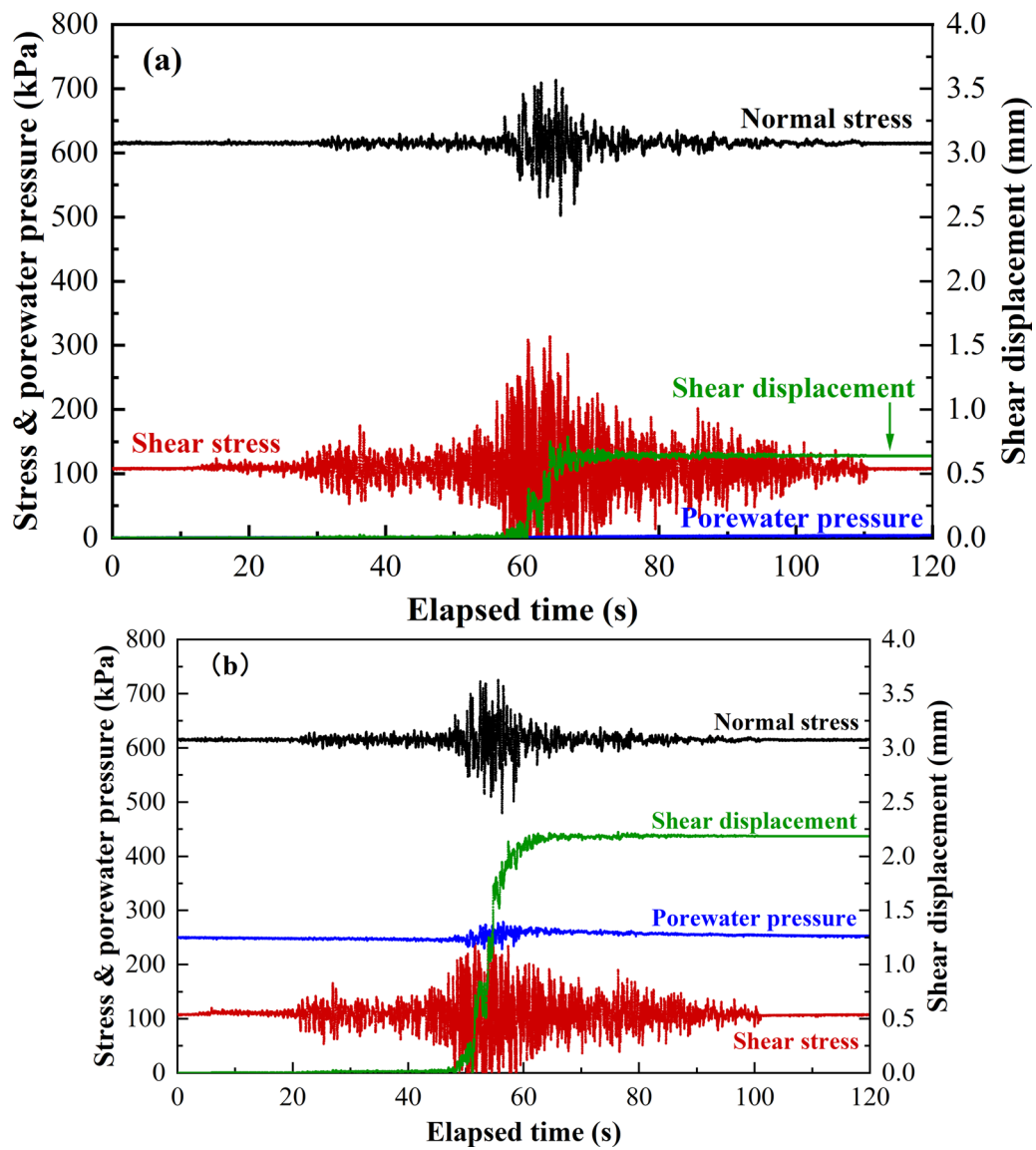


**Fig. 27** Time histories of normal and shear stresses, shear displacement and porewater pressure by ring shear test in non-porewater condition (a) and proposed 250-kPa-porewater condition (b)

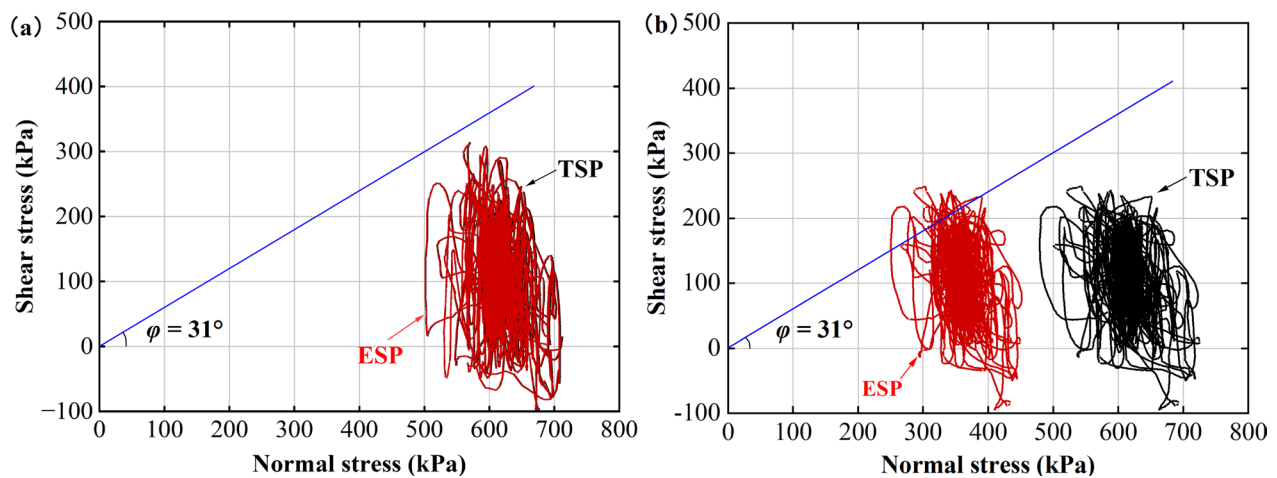


**Fig. 28** Stress path of the mudstone sample by ring shear test in non-porewater condition (a) and proposed 250-kPa-porewater condition (b). TSP and ESP represent total stress path and effective stress path, respectively. The blue line is shear strength line of the saturated sample by the shear ring test

#### Author contributions

Fawu Wang made the outline, and Kongming Yan prepared the original manuscript, while Masakatus Miyajima, Halil Kumsar, Ömer Aydan, Reşat Ulusay, Zhigang Tao and Fawu Wang refined it. Excepting Ye Chen, all authors conducted the field investigation collaboratively. Ye Chen conducted the ring shear tests and laboratory on the liquefaction samples. All authors read and approved the final manuscript.

#### Declarations

##### Competing interests

The authors declare that they have no competing interests.

Published online: 21 February 2024

#### References

- Aydan Ö (2023) Earthquake science and engineering (chapter 10: earthquake prediction). CRC Press, Boca Raton
- Aydan Ö, Ulusay R (2023) A quick report on Pazarcık and Ekinözü earthquake (Türkiye) of February 2023. [https://committees.jsce.or.jp/eec205/system/files/FINA\\_RU\\_OA\\_pazarcik\\_ekinozu\\_eqs\\_qr.pdf](https://committees.jsce.or.jp/eec205/system/files/FINA_RU_OA_pazarcik_ekinozu_eqs_qr.pdf)
- International Blue Crescent Relief and Development Foundation (IBC). Devastating Earthquakes in Southern Türkiye and Northern Syria, 18 May 2023, Situation Report 23 [EN/TR].
- ICRP of Cross-Fault Measurement for Earthquake Prediction, International Consortium on Geo-disaster Reduction, <http://www.icgdr.com/Home/Menu/310>, (accessed on 27 September, 2023)
- Norton M (2023) Active faults, surface ruptures and epicenters of the 2023 Turkey-Syria earthquake sequence

#### Publisher's Note

Springer Nature remains neutral with regard to jurisdictional claims in published maps and institutional affiliations.